

## CHANGES IN SOLAR ACTIVITY DURING THE WOLF MINIMUM—NEW INSIGHTS FROM A HIGH-RESOLUTION $^{14}\text{C}$ RECORD BASED ON DANISH OAK

Alexandra Fogtmann-Schulz<sup>1\*</sup>  • Claudia Baittinger<sup>2</sup> • Christoffer Karoff<sup>1,3,4</sup> • Jesper Olsen<sup>5,6</sup>  • Mads F Knudsen<sup>1,4</sup>

<sup>1</sup>Department of Geoscience, Aarhus University, Høegh-Guldbergs Gade 2, 8000 Aarhus, Denmark

<sup>2</sup>Environmental Archaeology and Materials Science, National Museum of Denmark, Copenhagen, Denmark

<sup>3</sup>Stellar Astrophysics Centre, Department of Physics and Astronomy, Aarhus University, Aarhus, Denmark

<sup>4</sup>CLIMATE Interdisciplinary Centre for Climate Change, Aarhus University, Roskilde, Denmark

<sup>5</sup>Aarhus AMS Centre (AARAMS), Department of Physics and Astronomy, Aarhus University, Aarhus, Denmark

<sup>6</sup>Centre for Urban Network Evolutions (UrbNet), Aarhus University, Aarhus, Denmark

**ABSTRACT.** We present a new biennial record of radiocarbon ( $^{14}\text{C}$ ) measured in Danish oak. The new record covers the years 1251–1378 CE, thereby spanning the Grand Solar Minimum known as the Wolf Minimum. Two oak samples from every other year were measured at the AMS facility at Aarhus University (Denmark), resulting in an average precision of 1.4‰ for the record. Spectral analysis of the new record revealed two peaks at 27 and 9.1 years, which could indicate the Hale cycle was lengthened and the Schwabe cycle shortened during the Wolf Minimum, but it is also possible that the amplitude of the Schwabe cycle was too small to be accurately identified with the acquired precision of this record. The record was bandpass filtered to investigate the variability of the amplitude in different bands, which showed a dampening of the amplitude during the second half of the Wolf Minimum in bands centered on the Schwabe and the Hale cycle, respectively. A reconstruction of the solar modulation function,  $\Phi$ , also showed a periodicity of ca. 9 years, and indicated that the Wolf Minimum was preceded by one cycle of decreased solar activity.

**KEYWORDS:** AMS dating, carbon, dating, radiocarbon, radiocarbon AMS dating.

### INTRODUCTION

In recent years, an increasing number of annually resolved radiocarbon ( $^{14}\text{C}$ ) records from tree rings have been published (e.g. Miyahara et al. 2006; Eastoe et al. 2019; Fogtmann-Schulz et al. 2019; Kudsk et al. 2019). These high-precision datasets make it possible to investigate the occurrence of high-frequency cyclicities in solar activity, including the Schwabe (ca. 11 years) and Hale (ca. 22 years) cycles. The behavior of these cycles during Grand Solar Minima (GSMs) are of particular interest, as they have important bearings on our understanding of the solar dynamo. A GSM is a time interval characterized by lower solar magnetic activity than usual over a period of 30–160 years (Usoskin et al. 2016). The Maunder Minimum (1640–1720 CE, timing from Usoskin et al. 2016) is the only GSM which is covered by direct observations of sunspots. These observations show that the sunspots almost completely disappeared during the Maunder Minimum (Eddy 1976). For the period prior to the invention of the telescope in 1610 CE, the documentation of GSMs relies on indirect proxies of solar activity. Since  $^{14}\text{C}$  is formed in the atmosphere as a product of incoming cosmic rays, the production rate of  $^{14}\text{C}$  is correlated with the strength of the geomagnetic as well as the solar magnetic fields, which both shield the Earth from cosmic rays. The strength of the magnetic fields changes the cut-off rigidity necessary for cosmic rays to penetrate the atmosphere of the Earth. Since the geomagnetic field changes on millennial timescales (Dutta 2016), it can be regarded as stable on shorter timescales. Changes on a timescale of <100 years are therefore primarily due to changes in the solar magnetic field.

\*Corresponding author. Email: [alfosc@geo.au.dk](mailto:alfosc@geo.au.dk).

The  $^{14}\text{C}$  produced in the atmosphere is mixed with the stable carbon isotopes,  $^{12}\text{C}$  and  $^{13}\text{C}$ , and becomes part of the carbon cycle, where it eventually will be taken up in terrestrial archives, such as trees. The age of tree rings can be independently determined by dendrochronology, which makes  $^{14}\text{C}$  in tree rings an ideal proxy for solar activity. However, since the precision of the accelerator mass spectrometry (AMS) measurements are of the same magnitude (2–3‰) as variations in atmospheric  $^{14}\text{C}$  associated with the Schwabe solar cycle (Stuiver and Braziunas 1993; Baroni et al. 2011), it is difficult to resolve past changes in the solar cycle.

Several GSMs have been identified since the use of indirect proxies for solar magnetic activity began. Stuiver and Quay (1980) named the interval from 1282 to 1342 CE the Wolf Minimum, which was characterized by a maximum in  $^{14}\text{C}$  near 1340 CE, based on measurements of  $^{14}\text{C}$  in tree-ring samples that each spanned 10 years. Usoskin et al. (2016) reconstructed the solar activity over the last nine thousand years based on  $^{10}\text{Be}$  and  $^{14}\text{C}$  records, and they identified the Wolf Minimum as spanning the years from 1270 to 1350 CE.

Hong et al. (2013), and Eastoe et al. (2019) have published annually resolved  $^{14}\text{C}$  records based on tree rings covering the Wolf Minimum. Hong et al. (2013) found peaks in a power spectrum of their annual dataset at 10.9 and 23.9 years corresponding to the Schwabe and Hale cycles, respectively. However, these periodicities were determined using the whole record spanning the years from 1250 to 1650 CE, and therefore it is unknown if these periodicities changed during the Wolf Minimum. The annual record of Eastoe et al. (2019) covered the years 998–1510 CE, and a spectral analysis of the whole record showed a peak corresponding to the Schwabe cycle at 10.4 years. The temporal evolution of the periodicities was investigated in a spectrogram, and in the time interval associated with the Wolf Minimum, there were indications of periodicities of 13.6 years and 26.4 years. More detailed information on the solar variability during the Wolf Minimum is needed to understand changes in the solar-cycle behavior during this GSM, and to resolve similarities and differences in solar activity among the different GSMs.

Eddy (1976) noted that the Spörer (1390–1550 CE, Usoskin et al. 2016) and Maunder minima occurred at the time of the two most severe temperature decreases during the Little Ice Age (LIA), which was an unusually cold time period between ca. 1350 and 1850 CE (Brönnimann et al. 2019), suggesting a relation between decreased solar activity and lower temperatures during the LIA. The exact definition of the LIA varies from study to study. Nagaya et al. (2012) suggested that the occurrence of the Wolf Minimum followed by the Spörer and Maunder minima could all have contributed to the lower than usual temperatures during the LIA, but the underlying mechanism and degree of causality remain uncertain. However, the timing of the Wolf Minimum does not coincide with that of the LIA. Instead, the beginning of the Wolf Minimum occurs at the end of the Medieval Climate Anomaly (950–1250 CE, Mann et al. 2009), which could suggest the Wolf Minimum instead contributed to ending the Medieval Climate Anomaly. This coincidence between changes in climate and GSMs is intriguing and more knowledge about solar activity during this period could help provide a better understanding of the relationship between solar activity and the climate on Earth, and elucidate if the correlation between GSMs and climate changed over time.

In this paper, we present a new biennial  $^{14}\text{C}$  record based on measurements of tree rings from Danish oak covering the interval 1251–1378 CE. We compare the new results to the

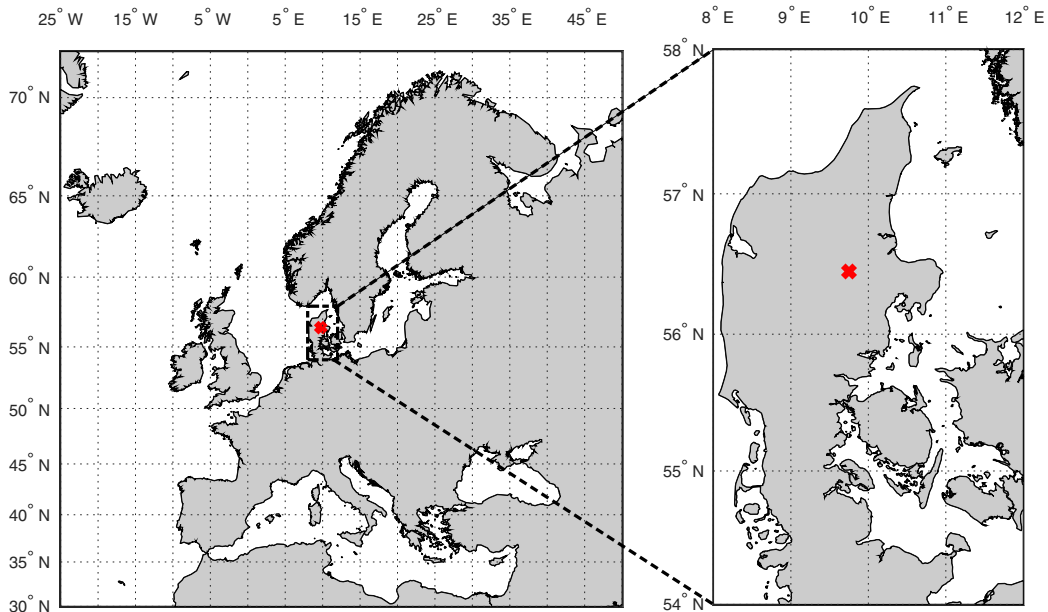


Figure 1 The red cross marks the location of the oak sample used for this study. (Please see electronic version for color figures.)

two above-mentioned annual records and perform frequency analysis to identify possible periodicities in the dataset. We also reconstruct the solar modulation potential across the Wolf Minimum, and compare it to the Spörer, Maunder, and Dalton minima.

## METHOD

Eighteen archaeological samples of oak (*Quercus* sp.) found at Skjern Slot (Bjerringbro, Mid Jutland, Denmark, 56.45°N, 9.75°E, see Figure 1) were dated using dendrochronology (Bonde and Eriksen 2003). The 18 tree-ring sequences were averaged to form a site chronology (7044i001) ranging from 1239 to 1477 CE. This curve was crossdated with master chronologies from Jutland using the program DENDRO for Windows (Tyers 1999) following the methods outlined by Baillie and Pilcher (1973). The master chronology best matching the Skjern Slot site chronology was that of Eastern Jutland (6m100001) with a  $t$  value of 11.11, thus validating the dendrochronological dates (Bonde and Eriksen 2003).

One of the 18 wood samples (70441029, G615, sample 2, hereafter referred to as SK2) with a tree-ring range of 1250–1425 CE was selected for AMS  $^{14}\text{C}$  dating. Individual ring widths of SK2 can be seen in Table S1 in the supplementary information. The tree-rings from 1250–1380 CE were separated into annual samples of early wood (EW) and late wood (LW) under a microscope using a surgeon scalpel. The LW samples from every second year were chosen for further analysis, as LW in oak has been shown to be a more robust recorder of past changes in the atmospheric radiocarbon levels than EW (Fogtmann-Schulz et al. 2017; Kudsk et al. 2018), in part because EW may contain radiocarbon from the previous growth season (McDonald et al. 2019).

The chosen LW samples were further pretreated to  $\alpha$ -cellulose following the procedure described in Fogtmann-Schulz et al. (2020), based on the method of Southon and Magana (2010). First, lignin was removed by treating with  $\text{NaClO}_2$  and HCl (2 times, 3 hr each, 70°C). After rinsing with 70°C milli-Q water, hemicelluloses were removed by treating with 17% NaOH (1 hr, room temperature). Lastly, after another rinse with 70°C milli-Q water, the samples were treated with 1 M HCl (30 min, 70°C) to remove any  $\text{CO}_2$  absorbed from the atmosphere during the step with the base treatment. The samples were then carefully rinsed with milli-Q water and freeze-dried.

The resulting  $\alpha$ -cellulose fraction of the initial wood sample was in the range 32.2% to 48.8%, with most samples around 40%. According to Miller (1999), cellulose constitutes approximately 50% of wood substance in general, implying all samples experienced some loss of material. This was inevitable, especially during transfer of the sample from the glass vials used during pretreatment to the tube used for freeze-drying.

Next, the  $\alpha$ -cellulose samples were prepared for measurement on an AMS system. The samples were first combusted to  $\text{CO}_2$  with CuO in sealed glass tubes. Then, the  $\text{CO}_2$  samples were purified and graphitized using the procedure of Olsen et al. (2017). The radiocarbon fraction was then measured using a 1 MV HVEE Tandem AMS system at Aarhus AMS Centre (AARAMS) at Aarhus University, Denmark (Olsen et al. 2017). To correct the measured  $^{14}\text{C}/^{12}\text{C}$  ratios for isotopic fractionation, the  $^{13}\text{C}/^{12}\text{C}$  ratio was measured online in the AMS system and subsequently normalized to a standard  $\delta^{13}\text{C}$  value of  $-25\text{‰}$  Vienna Pee Dee Belemnite (Stuiver and Polach 1977). The resulting radiocarbon ages are reported as conventional  $^{14}\text{C}$  dates in  $^{14}\text{C}$  years BP (Before Present = 1950 CE). Also reported are  $\Delta^{14}\text{C}$  values, which are calculated and age-corrected according to Stuiver and Polach (1977) and Jull et al. (2014).

The measured samples covered the timespan 1251–1378 CE, with two samples measured for every second year. To avoid using very narrow tree rings, uneven years were measured in the interval 1251–1367 CE, and even years were measured in the interval 1368–1378 CE. A total of 137 samples were measured from 65 individual LW tree rings.

The two individual measurements from the same year were combined by calculating a weighted mean for the samples that passed a reduced  $\chi^2$  test. Seven years failed the  $\chi^2$  test, and one extra sample was therefore measured for each of these years. The  $\chi^2$  test was repeated for the 3 samples from the same year, but 6 of the 7 years still failed the test. A weighted mean was calculated for the one year that passed the test. For 5 of the remaining 6 years, the measurement with the greatest distance to the mean divided by the uncertainty was deemed an outlier. For the last year that failed the test, none of the individual measurements could clearly be deemed an outlier, and instead, the uncertainty was enhanced by multiplying with the square root of the  $\chi^2$  value.

The resulting dataset was filtered with an infinite impulse-response low-pass filter with a stopband attenuation of 60 dB and a cut-off frequency of  $1/5 \text{ yr}^{-1}$  to reduce the year-to-year scatter and help identify long-term changes. The dataset was also filtered using a range of different bandpass filters, including (i) a filter with pass band frequencies of  $1/40$ – $1/16 \text{ yr}^{-1}$  to study the Hale solar cycle, (ii) a filter with pass band frequencies corresponding to  $1/16$ – $1/7.1 \text{ yr}^{-1}$  to study the Schwabe solar cycle, and a filter with pass band frequencies of  $1/7.1$ – $1/4.05 \text{ yr}^{-1}$  to study other variabilities with higher frequencies. All the bandpass filters were sixth-order butterworth filters.

Furthermore, the dataset was analyzed with a Lomb-Scargle Fourier Transformation to identify the presence of significant periodicities. This was done using REDFIT (Schulz and Mudelsee 2002), which calculated a power spectrum for the measured data and identified false-alarm levels based on comparison with red-noise data. The long-term variations in the dataset were removed prior to this analysis by subtracting a 34-yr moving mean.

In order to study variations of the solar magnetic field, we reconstructed the solar modulation function,  $\Phi$ . First, the biennial data were linearly interpolated to a resolution of 0.1 yr. Next, the data were filtered with a lowpass filter with a cut-off frequency of  $1/8 \text{ yr}^{-1}$ , and inserted into a carbon box model (Muscheler et al. 2005) to model changes in the  $^{14}\text{C}$  production rate. The IntCal20 data (Reimer et al. 2020) were used in the interval from 10,000 BP to 1250 CE and from 1379 CE to 1800 CE to better constrain the box model in time intervals where we have no data. The modeled  $^{14}\text{C}$  production rate was combined with reconstructions of the geomagnetic field strength by Knudsen et al. (2008) to estimate  $\Phi$  (Masarik and Beer 1999). In order to estimate the uncertainty of  $\Phi$ , the original  $\Delta^{14}\text{C}$  data were resampled 10,000 times using a normal distribution defined by the value and standard deviation of each  $\Delta^{14}\text{C}$  data point. The calculation of  $\Phi$  was then repeated for each resampling. The final  $\Phi$  estimate associated with each year was defined by the mean and standard deviation of these 10,000 values.

## RESULTS

The average precision of the individual  $\Delta^{14}\text{C}$  measurements (Table S2 in the supplementary information) is  $\pm 1.9\%$ , equivalent to  $\pm 16$   $^{14}\text{C}$  years. The combination of 2 or 3 measurements from the same year (Figure 2 and Table S2) yields a combined precision of  $\pm 1.4\%$ , equivalent to  $\pm 11$   $^{14}\text{C}$  years.

There is a general positive offset of  $2.76 \pm 0.23\%$  between the new SK2 dataset from Danish oak and the IntCal20 curve (Reimer et al. 2020) (Figure 2). A  $\chi^2$  test of these two datasets failed, indicating that they are statistically different or the estimated errors are too small ( $\chi^2: 2.03 \leq 1.31$ ). The offset is largest for the early part of the record, whereas it becomes negligible after 1345 CE (Figure 2). When the samples were measured in the AMS, they were mixed in the different machine runs, i.e. they were not measured chronologically. Furthermore, there is nothing in the machine performance that suggests that these measurements were contaminated, the standard and background values were comparable to normal laboratory values.

Our SK2 dataset and the annual dataset of Hong et al. (2013) have 65 years in common. Out of these 65 years, 22 years fail a  $\chi^2$  test, implying they are statistically different and cannot be combined. The average difference in  $\Delta^{14}\text{C}$  values between these two datasets is  $3.74 \pm 0.51\%$  ( $\chi^2: 3.60 \leq 1.31$ ). Hong et al. (2013) noted an average offset of  $+40.0$   $^{14}\text{C}$  years (i.e. older ages) compared to the IntCal04 data (Reimer et al. 2004) for the period 1330 to 1430 CE. However, they did not provide an explanation for this offset. When comparing the Hong et al. (2013) data to the IntCal20 data (Reimer et al. 2020) for the time period 1330–1430 CE, the offset is  $+36 \pm 3$   $^{14}\text{C}$  years, equivalent to  $4.52 \pm 0.41\%$ . When subtracting the mean offset between the SK2 dataset and the Hong dataset, and repeating the  $\chi^2$  test, 16 of the 65 years in common fail the test. We also subtracted a 35-year running mean from both datasets and repeated the  $\chi^2$  test. This resulted in 14 failed years out of 65 years in common. The Hong dataset has an average precision of 32  $^{14}\text{C}$  years, i.e. more than three

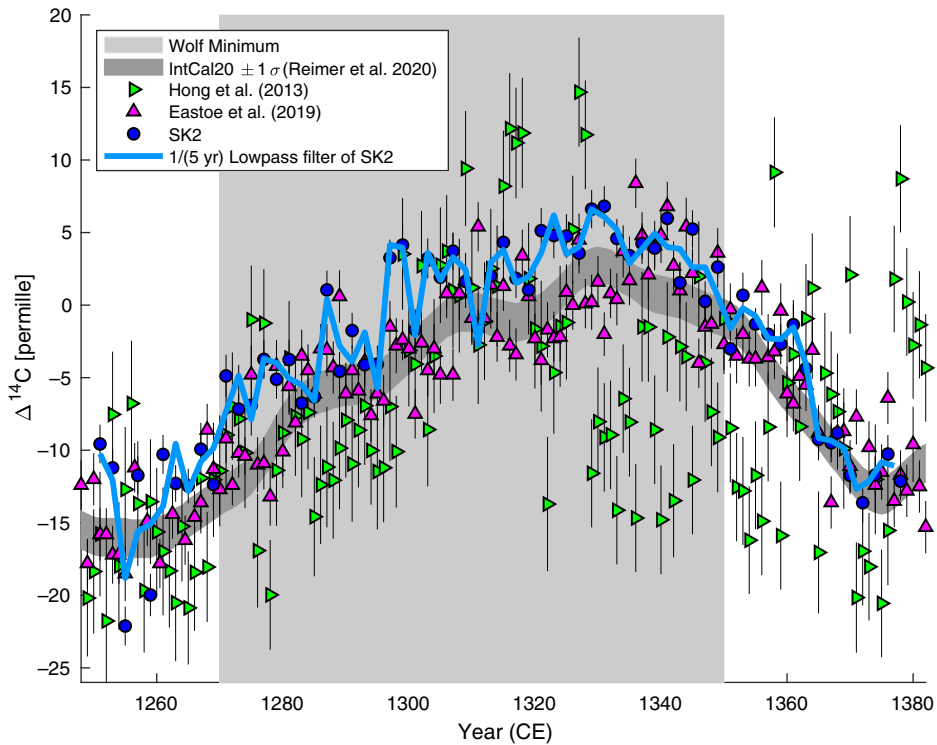


Figure 2 The  $\Delta^{14}\text{C}$  record from this study is shown with blue circles. A lowpass filter with cut off frequency of  $1/(5 \text{ yr})$  is shown for visual clarification with a light blue line. Data from Hong et al. (2013) are shown with green triangles, and data from Eastoe et al. (2019) are shown with magenta triangles. The data from IntCal20 (Reimer et al. 2020) are shown as a dark grey band including  $1 \sigma$  error. The light grey box marks the interval of the Wolf Minimum (1270–1350 CE; Usoskin et al. 2016).

times higher than the average precision obtained in this study for the SK2 dataset when 2–3 samples are combined, and it also displays larger variability. To get a measure of the variability, we calculated the standard deviation of the difference between the sample values and a running mean (for 10 years) of the dataset. For the Hong dataset, this resulted in a variability of 5.4‰, whereas it is only 2.4‰ for the SK2 dataset. The larger variability associated with the Hong dataset, which possibly reflect local conditions and/or differences in wood cutting and measurement procedures, may explain the high number of years failing a  $\chi^2$  test.

The annual dataset of Eastoe et al. (2019) has 59 years in common with our SK2 dataset. Out of these 59 years, 17 fail a  $\chi^2$  test and are therefore statistically different. The average offset between these two datasets is  $2.02 \pm 0.29\text{‰}$  ( $\chi^2$ :  $2.69 \leq 1.32$ ). When this mean offset is subtracted from the data, 13 of the 59 years in common fail a  $\chi^2$  test. If we subtract a 35-year running mean from both datasets, 11 of 59 years in common fail the test. This implies that our SK2 dataset is statistically different from the two existing annually resolved contemporaneous records based on  $\chi^2$  tests, or that the associated errors are underestimated.

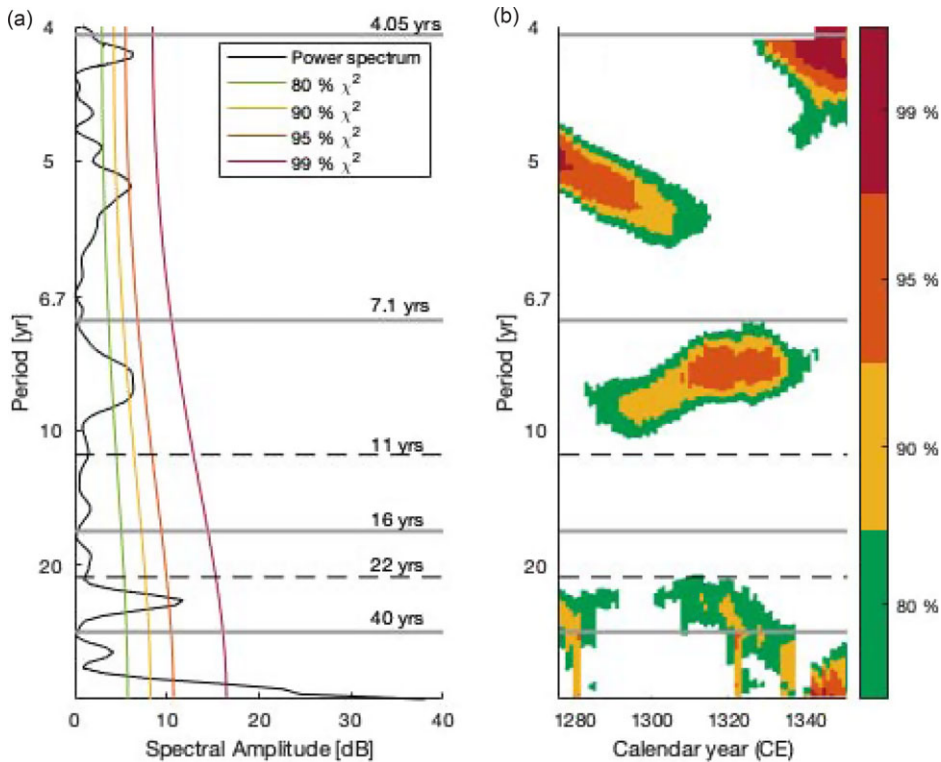


Figure 3 Amplitude spectrum (a) and time-resolved periodogram (b) of our data (black). The first and last 25 years are missing in the periodogram due to a window size of 50 years. A 34-year running mean filter has been subtracted from the data prior to these calculations. The black, dashed, horizontal lines mark periods of 11 and 22 years, respectively. The four grey horizontal lines mark the boundaries of the bandpass filters used in Figure 4 (4.05, 7.1, 16, and 40 years).

The variability of  $\Delta^{14}\text{C}$  over time is investigated with an amplitude spectrum (Figure 3A). This shows a peak corresponding to a period of 27 years above the 95% false-alarm level. There are furthermore two peaks above the 95% false-alarm level at 5.3 and 4.2 years. One peak additionally rises above the 90% false-alarm level at 9.1 years, but this is the only peak found near the 11-yr Schwabe cycle. The time evolution of these periodicities is visualized in a periodogram (Figure 3B). The periodicity around 9 years is present throughout most of the investigated time period, from ca. 1280 to 1340 CE, whereas the periodicity around 27 years is not significant between ca. 1290 and 1300 CE, indicating that this cyclicity weakened during part of the Wolf Minimum.

The variability of  $\Delta^{14}\text{C}$  is further investigated by applying different bandpass filters to the SK2 time series (Figure 4). In all the different bands, the amplitude is highest before and during the first half of the Wolf Minimum (1250–1310 CE). In the bandpass centered on the Hale cycle (16–40 years), the variability is greatly dampened from 1320 CE until the end of the time series (Figure 4C). A similar pattern is observed for the variability in the bandpass centered on the Schwabe cycle (7.1–16 years) (Figure 4B). A minimum amplitude is reached between 1345 and 1365 CE. The variability in the bandpass with periods of 4.05–7.1 years is also lowest after 1310 CE (Figure 4A). This high-frequency variability is

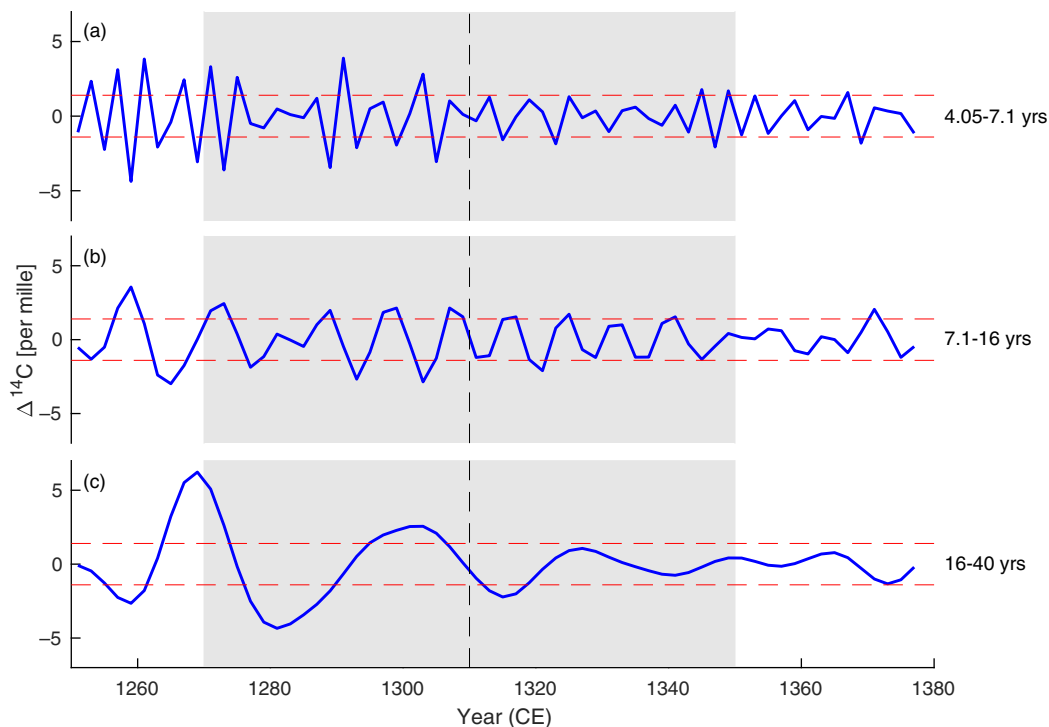


Figure 4 Bandpass filtered  $\Delta^{14}\text{C}$  data. The different bands are confined by the periods written on the right side. The grey box marks the duration of the Wolf Minimum according to Usoskin et al. (2016). The dashed black line marks the center year (1310 CE). The dashed red lines are plotted at  $\pm 1.4\text{‰}$ , marking the average precision of these measurements.

of the same magnitude as the variability in the Schwabe- and Hale-centered bands during the Wolf Minimum.

The reconstructed solar modulation function,  $\Phi$ , is shown in Figure 5. One cycle from 1250 to 1260 CE, characterized by a large magnitude, is followed by several cycles of reduced magnitude until 1360 CE. Thereafter, the magnitude of the cycles becomes larger again. The minima of the cycles before the Wolf Minimum (in 1250–1270 CE) are higher than the cycle minima during most of the Wolf Minimum (in 1270–1340 CE), whereas the cycle-minima values become larger towards the end of the Wolf Minimum (from 1340 CE onwards). A clear cyclicity with a duration between 8 and 10 years is evident in these data, particularly during the Wolf Minimum. The data were lowpass filtered with a cut-off frequency of  $1/8 \text{ yr}^{-1}$  prior to the calculation of  $\Phi$ , which makes the ca. 9-yr periodicity stand out more clearly than in the original data.

## DISCUSSION

The reconstruction of the solar modulation function,  $\Phi$ , shows lowered solar activity during the Wolf Minimum. Vaquero et al. (2011) suggested the Maunder Minimum was preceded by two solar cycles of reduced activity, indicating a gradual transition into the Grand Minimum. Our reconstruction of  $\Phi$  showed that the cycle from 1260 to 1270 CE, i.e. one cycle before the onset of the Wolf Minimum according to the definition of Usoskin et al. (2016), was of similar

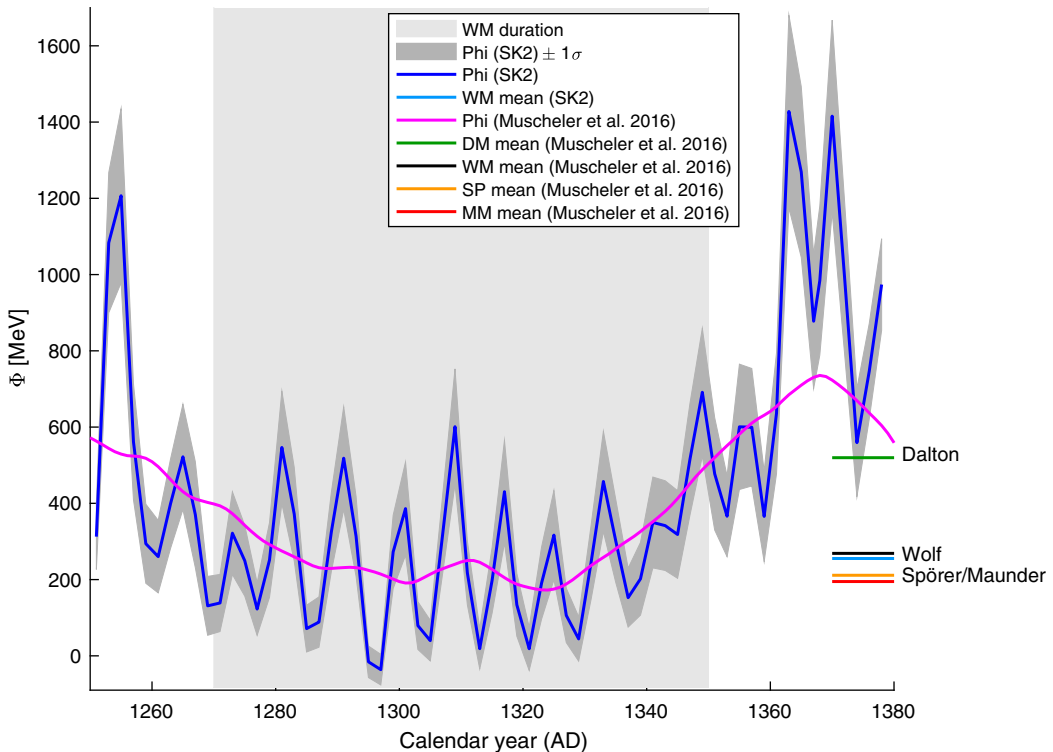


Figure 5 Solar modulation function,  $\Phi$ , reconstructed from the filtered radiocarbon record in blue. The grey band marks the standard deviation found by resampling the  $\Delta^{14}\text{C}$  values 10,000 times and calculating  $\Phi$  for each resampling of the signal.  $\Phi$  values based on  $^{14}\text{C}$  from Muscheler et al. (2016) is shown in magenta. The light grey box mark the duration of the Wolf Minimum according to Usoskin et al. (2016). On the right side, the mean values of  $\Phi$  during the Dalton Minimum (DM), Maunder Minimum (MM), Spörer Minimum (SM), and Wolf Minimum (WM) from the Muscheler et al. (2016) reconstruction is shown as well as the mean value of  $\Phi$  during the Wolf Minimum based on the SK2 reconstruction.

amplitude as the following cycles that fall within the Wolf Minimum. This cycle could be a transitioning cycle, as suggested by Vaquero et al. (2011).

The mean value of the reconstructed  $\Phi$  during the Wolf Minimum (1270–1350 CE) is  $255 \pm 177$  MeV. Muscheler et al. (2016) reconstructed the solar modulation function based on the IntCal13 record for the northern (Reimer et al. 2013) and southern hemispheres (Hogg et al. 2013), as well as the annual radiocarbon record of Stuiver et al. (1998) covering the last ca. 500 years. Their approach to calculating  $\Phi$  was similar to the approach used in this paper, but the filter they applied was different. This reconstruction of  $\Phi$  is shown in Figure 5. The mean value of  $\Phi$  during the Wolf Minimum in the record of Muscheler et al. (2016) was  $269 \pm 81$  MeV, which is consistent with the result from this paper. We also calculated the mean value of  $\Phi$  based on the reconstructed record presented in Muscheler et al. (2016) during the Spörer Minimum (1390–1550 CE), Maunder Minimum (1640–1720 CE), and Dalton Minimum (1790–1820 CE) (Figure 5). The mean value during the Dalton Minimum was  $520 \pm 205$  MeV, which is much higher than the mean value during the Wolf Minimum, revealing the Wolf Minimum to be considerably deeper than the Dalton Minimum. The mean values of  $\Phi$  during the Spörer and Maunder

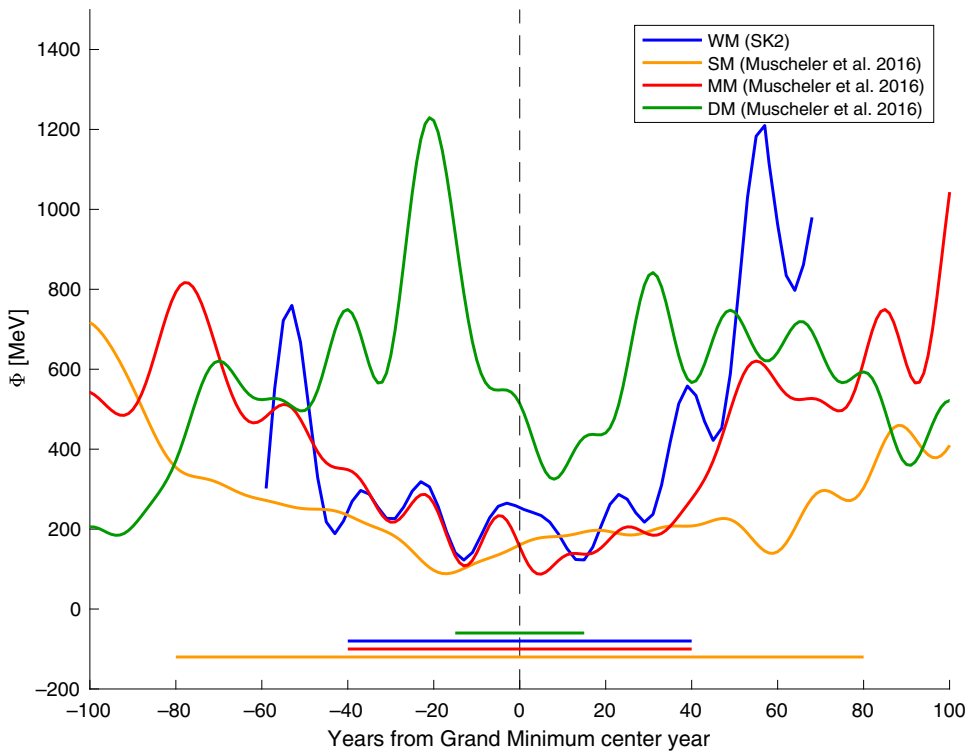


Figure 6 The solar modulation function,  $\Phi$ , during the four most recent GSMs: The Dalton Minimum (green), Maunder Minimum (red), Spörer Minimum (orange), and Wolf Minimum (blue) plotted with respect to their center year (timing according to Usoskin et al. 2016 and Usoskin et al. 2017), which is marked with a dashed, black, vertical line. The duration of the GSMs are marked with the horizontal lines in the bottom, the color corresponds to the color of the curve. The curves showing the Dalton, Maunder, and Spörer Minimum are the  $\Phi$  reconstruction from Muscheler et al. (2016) filtered with a lowpass filter with a cut-off frequency of  $1/16 \text{ yr}^{-1}$ . The curve showing the Wolf Minimum is the  $\Phi$  reconstruction from this paper (SK2) filtered by a lowpass filter with a cut-off frequency of  $1/16 \text{ yr}^{-1}$ .

minima were  $211 \pm 65 \text{ MeV}$  and  $195 \pm 71 \text{ MeV}$ , respectively, i.e. lower than the mean value during the Wolf Minimum. It is thus possible that the Wolf Minimum was different from the Maunder Minimum in the sense that sunspots may have occurred regularly during the Wolf Minimum, as oppose to the Maunder Minimum that was characterized by extended periods with no sunspots.

In order to compare the Wolf Minimum to the three subsequent GSMs, we plotted our record of  $\Phi$  together with the record of  $\Phi$  from Muscheler et al. (2016) across the Spörer, Maunder, and Dalton minima (Figure 6). The data were all lowpass filtered with a  $1/16 \text{ yr}^{-1}$  cut-off frequency to enable a better comparison of the overall shape of the different minima. The Dalton Minimum is clearly not as deep nor as long as the other minima. The Maunder Minimum is slightly deeper and wider than the Wolf Minimum, in part because the Wolf Minimum rises more steeply towards the end. The Spörer Minimum is of similar depth as the Maunder Minimum, but the duration of the Spörer Minimum is considerably longer. We note that the timespan officially associated with the Dalton Minimum (1790–1820 CE) seems misaligned with the  $\Phi$  reconstruction of Muscheler et al., although this misalignment

may partly relate to the filtering of the  $\Phi$  reconstruction. For a comparison of the  $\Delta^{14}\text{C}$  values across the Wolf, Spörer and Maunder minima, see Figure S1 in the supplementary material

The variability in  $\Delta^{14}\text{C}$  in two bands centered on the Schwabe and the Hale cycle, respectively, is higher in the first 40 years of the Grand Minimum than in the last 40 years, implying that the Wolf Minimum was asymmetric with respect to the radiocarbon variability, as also observed for the Spörer Minimum (Fogtmann-Schulz et al. 2019). This could indicate that the first half of a GSM has a slow decrease of amplitude until the overall minimum is reached, where after the amplitude rises more quickly to a non-GSM level. The variability in the band corresponding to periods of 4.05–7.1 years is of similar amplitude as the variability in the Schwabe band, and this makes it more difficult to detect the Schwabe cycle in the data. The exact cause of the 4–7-year variability is unknown, and we cannot rule out the possibility that it is strongly influenced by noise. However, Stuiver and Braziunas (1993) also found considerable variability in this period band (particularly around 5.1–6.4 years) in their  $\Delta^{14}\text{C}$  record from firs on the westcoast of the US. They suggested this variability was caused by changes in the ocean-atmosphere exchange associated with variations in upwelling related to the El Niño-Southern Oscillation (ENSO). Similarly, we propose that the 4–7-year variability in the SK2 dataset reflect changes in ENSO-related upwelling. It is also possible that changes in the ocean-atmosphere exchange related to the North Atlantic Oscillation contributed to the 4–7-year variability in the SK2 dataset. Olsen et al. (2012) found that the North Atlantic Oscillation (NAO) varied significantly with periodicities between 5 and 8 years in the past.

The power spectrum shows a peak at 27 years periodicity, being the only significant peak in the vicinity of the Hale cycle. Eastoe et al. (2019) also found a period of 26.4 years to be present in their annual  $^{14}\text{C}$  dataset around 1300–1330 CE, where after the period shortened between ca. 1330 and 1350 CE, and then returned to a period of 26.4 years from 1350 to 1375 CE. They also found some variability between ca. 1275 and 1325 CE with a period of ca. 13.6 years, but the amplitude was not high and the significance was not indicated.

Solanki et al. (2002), Miyahara et al. (2010), and Moriya et al. (2019) suggested that the Schwabe and Hale cycles lengthen during GSMs, which may also be the case in our record. However, the only significant peak close to the Schwabe cycle is the peak at 9.1 years, which may indicate the opposite, i.e. that the Schwabe cycle shortened during the GSM. Another possibility is that this is not the Schwabe cycle, in which case the amplitude of the Schwabe cycle must have been less than 1.4‰. The peak at 27 years may be the third harmonic of the 9.1-year periodicity, or it may be a lengthened Hale cycle.

## CONCLUSION

Changes in atmospheric radiocarbon across the Wolf Minimum have been investigated with a new biennially resolved  $\Delta^{14}\text{C}$  record based on tree rings from Danish oak. Spectral analysis of the new  $\Delta^{14}\text{C}$  record revealed significant peaks at ~5.5 years, 9.1 years, and 27 years. This suggests that either the Schwabe cycle was shortened during the Wolf Minimum, or, alternatively, that the Schwabe cycle had an amplitude that was too small to be accurately identified during the Wolf Minimum. In contrast, the 27-year periodicity indicates that the Hale cycle was lengthened during the Wolf Minimum. Alternatively, 27-year periodicity could represent the third harmonic of the 9.1 years periodicity. The bandpass-filtered record showed dampened amplitudes of variability during the second half of the Wolf

Minimum, and in the 30 years following the minimum in bands centred on the Schwabe and Hale cycles, respectively. Variations in  $\Delta^{14}\text{C}$  with a period of 5.5 years most likely reflect changes in ocean-atmosphere exchange related to ENSO and the NAO.

A reconstruction of the solar modulation function showed a clear ca. 9-year period of variability, but also indicates that the interval characterized by low amplitudes began already in 1260 CE, implying that there was a gradual transition into the Wolf Minimum with one cycle of reduced activity preceding the GSM.

A comparison of the solar modulation function during the Wolf Minimum with similar reconstructions covering the Spörer, Maunder, and Dalton minima showed that the Wolf Minimum resembles the Maunder Minimum with respect to duration and depth. The Wolf Minimum was deeper than the Dalton Minimum, but it was not quite as deep as the Maunder Minimum. However, the variability changes associated with the bandpass-filtered record resemble the variability during the Spörer Minimum more than the Maunder Minimum.

## ACKNOWLEDGMENTS

We would like to acknowledge financial support from the Villum Foundation (VKR023114 and VKR010116). Funding for the Stellar Astrophysics Centre is provided by the Danish National Research Foundation (Grant Agreement DNRF106). We thank the staff at AARAMS for help with the laboratory work. We would also like to thank Raimund Muscheler for help with the carbon box model.

## SUPPLEMENTARY MATERIAL

To view supplementary material for this article, please visit <https://doi.org/10.1017/RDC.2020.126>

## REFERENCES

- Baillie MGL, Pilcher JR. 1973. A simple crossdating program for tree-ring research. *Tree-Ring Bulletin* 33:7–14.
- Baroni M, Bard E, Petit J-R, Magand O, Bourlès D. 2011. Volcanic and solar activity, atmospheric circulation influences on cosmogenic  $^{10}\text{Be}$  fallout at Vostok and Concordia (Antarctica) over the last 60 years. *Geochimica et Cosmochimica Acta* 75:7132–7145. doi: [10.1016/j.gca.2011.09.002](https://doi.org/10.1016/j.gca.2011.09.002).
- Bonde N, Eriksen OH. 2003. Skjern Slot, Viborg Amt. Dendrokronologisk Laboratorium, NNU Rapport 1. [http://www.nnuweb.dk/dendro/nnu1\\_03.htm](http://www.nnuweb.dk/dendro/nnu1_03.htm).
- Brönnimann S, Franke J, Nussbaumer SU, Zumbühl HJ, Steiner D, Trachsel M, Hegerl GC, Schurer A, Worni M, Malik A, Flückiger J, Raible CC. 2019. Last phase of the Little Ice Age forced by volcanic eruptions. *Nature Geoscience* 12(8):650–656. doi: [10.1038/s41561-019-0402-y](https://doi.org/10.1038/s41561-019-0402-y).
- Dutta K. 2016. Sun, ocean, nuclear bombs, and fossil fuels: Radiocarbon variations and implications for high-resolution dating. *Annual Review of Earth and Planetary Sciences* 44 (1):239–275. doi: [10.1146/annurev-earth-060115-012333](https://doi.org/10.1146/annurev-earth-060115-012333).
- Eastoe CJ, Tucek CS, Touchan R. 2019.  $\Delta^{14}\text{C}$  and  $\Delta^{13}\text{C}$  in annual tree-ring samples from *Sequoiadendron Giganteum*, AD 998–1510: solar cycles and climate. *Radiocarbon* 61 (3): 661–680. doi: [10.1017/rdc.2019.27](https://doi.org/10.1017/rdc.2019.27).
- Eddy JA. 1976. The Maunder Minimum. *Science* 192(4245):1189–1202.
- Fogtmann-Schulz A, Kudsk SGK, Trant PLK, Baittinger C, Karoff C, Olsen J, Knudsen MF. 2019. Variations in solar activity across the Spörer Minimum based on radiocarbon in Danish oak. *Geophysical Research Letters* 46(15): 8617–8623. doi: [10.1029/2019GL083537](https://doi.org/10.1029/2019GL083537).
- Fogtmann-Schulz A, Østbø SM, Nielsen SGB, Olsen J, Karoff C, Knudsen MF. 2017. Cosmic ray event in 994 C.E. recorded in radiocarbon from Danish oak. *Geophysical Research Letters* 44: 8621–8628. doi: [10.1002/2017GL074208](https://doi.org/10.1002/2017GL074208).
- Fogtmann-Schulz A, Kudsk SGK, Adolphi F, Karoff C, Knudsen MF, Loader NJ, Muscheler R, Trant PLK, Østbø SM, Olsen J. 2020. Batch

- processing of tree ring samples for radiocarbon analysis. *Radiocarbon*:1–13. doi: [10.1017/RDC.2020.119](https://doi.org/10.1017/RDC.2020.119).
- Hogg AG, Hua Q, Blackwell PG, Niu M, Buck CE, Guilderson TP, Heaton TJ, Palmer JG, Reimer PJ, Reimer RW, Turney CSM, Zimmerman SRH. 2013. SHCal13 Southern Hemisphere calibration, 0–50,000 years cal BP. *Radiocarbon* 55(4):1889–1903. doi: [10.2458/azu\\_js\\_rc.55.16783](https://doi.org/10.2458/azu_js_rc.55.16783).
- Hong W, Park JH, Park WK, Sung KS, Lee KH, Park G, Kim YE, et al. 2013. Calibration curve from AD 1250 to AD 1650 by measurements of tree-rings grown on the Korean Peninsula. *Nuclear Instruments and Methods in Physics Research, Section B: Beam Interactions with Materials and Atoms* 294:435–439. doi: [10.1016/j.nimb.2012.08.041](https://doi.org/10.1016/j.nimb.2012.08.041).
- Jull AJT, Panyushkina IP, Lange TE, Kukarskih VV, Myglan VS, Clark KJ, Salzer MW, Burr GS, Leavitt SW. 2014. Excursions in the  $^{14}\text{C}$  record at A.D. 774–775 in tree rings from Russia and America. *Geophysical Research Letters* 41:3004–3010. doi: [10.1002/2014GL059874](https://doi.org/10.1002/2014GL059874).
- Knudsen MF, Risager P, Donadini F, Snowball I, Muscheler R, Korhonen K, Pesonen LJ. 2008. Variations in the geomagnetic dipole moment during the Holocene and the past 50 kyr. *Earth and Planetary Science Letters* 272:319–329.
- Kudsk SGK, Olsen J, Nielsen LN, Fogtmann-Schulz A, Knudsen MF, Karoff C. 2018. What is the carbon origin of early wood? *Radiocarbon* 60(5):1457–1464. doi: [10.1017/RDC.2018.97](https://doi.org/10.1017/RDC.2018.97).
- Kudsk SGK, Philippsen B, Baittinger C, Fogtmann-Schulz A, Knudsen MF, Karoff C, Olsen J. 2019. New single-year radiocarbon measurements based on Danish oak covering the periods AD 692–790 and 966–1057. *Radiocarbon* 62(4). doi: [10.1017/rdc.2019.107](https://doi.org/10.1017/rdc.2019.107).
- Mann ME, Zhang Z, Rutherford S, Bradley RS, Hughes MK, Shindell D, Ammann C, Faluvegi G, Ni F. 2009. Global signatures and dynamical origins of the Little Ice Age and Medieval Climate Anomaly. *Science* 326(5957):1256–1260. doi: [10.1126/science.1177303](https://doi.org/10.1126/science.1177303).
- Masarik J, Beer J. 1999. Simulation of particle fluxes and cosmogenic nuclide production in the Earth's atmosphere. *Journal of Geophysical Research* 104(D10):12099–12111. <http://onlinelibrary.wiley.com/doi/10.1029/1998JD200091/full>.
- McDonald L, Chivall D, Miles D, Bronk Ramsey C. 2019. Seasonal variations in the  $^{14}\text{C}$  content of tree rings: influences on radiocarbon calibration and single-year curve construction. *Radiocarbon* 61(1):185–194. doi: [10.1017/rdc.2018.64](https://doi.org/10.1017/rdc.2018.64).
- Miller RB. 1999. Structure of wood. In: *Wood handbook: wood as an engineering material*, 2.1–2.5. Madison (WI): USDA Forest Service, Forest Products Laboratory.
- Miyahara H, Masuda K, Muraki Y, Kitagawa H, Nakamura T. 2006. Variation of solar cyclicity during the Spoerer Minimum. *Journal of Geophysical Research* 111(A03103). doi: [10.1029/2005JA011016](https://doi.org/10.1029/2005JA011016).
- Miyahara H, Kitazawa K, Nagaya K. 2010. Is the Sun heading for another Maunder Minimum? Precursors of the Grand Solar Minima. *Journal of Cosmology* 8:1970–1982.
- Moriya T, Miyahara H, Ohyama M, Hakozaiki M, Takeyama M, Sakurai H, Tokanai F. 2019. A study of variation of the 11-yr solar cycle before the onset of the Spoerer Minimum based on annually measured  $^{14}\text{C}$  content in tree rings. *Radiocarbon* 61 (6):1749–1754. doi: [10.1017/RDC.2019.123](https://doi.org/10.1017/RDC.2019.123).
- Muscheler R, Beer J, Kubik PW, Synal HA. 2005. Geomagnetic field intensity during the last 60,000 years based on  $^{10}\text{Be}$  and  $^{36}\text{Cl}$  from the Summit Ice Cores and  $^{14}\text{C}$ . *Quaternary Science Reviews* 24(16–17):1849–1860. doi: [10.1016/j.quascirev.2005.01.012](https://doi.org/10.1016/j.quascirev.2005.01.012).
- Muscheler R, Adolphi F, Herbst K, Nilsson A. 2016. The revised sunspot record in comparison to cosmogenic radionuclide-based solar activity reconstructions. *Solar Physics* 291(9–10):3025–3043. doi: [10.1007/s11207-016-0969-z](https://doi.org/10.1007/s11207-016-0969-z).
- Nagaya K, Kitazawa K, Miyake F, Masuda K, Muraki Y, Nakamura T, Miyahara H, Matsuzaki H. 2012. Variation of the Schwabe cycle length during the Grand Solar Minimum in the 4th century BC deduced from radiocarbon content in tree rings. *Solar Physics* 280(1):223–236. doi: [10.1007/s11207-012-0045-2](https://doi.org/10.1007/s11207-012-0045-2).
- Olsen J, Anderson NJ, Knudsen MF. 2012. Variability of the North Atlantic Oscillation over the past 5,200 years. *Nature Geoscience* 5(11):808–812. doi: [10.1038/ngeo1589](https://doi.org/10.1038/ngeo1589).
- Olsen J, Tikhomirov D, Groesen C, Heinemeier J, Klein M. 2017. Radiocarbon analysis on the new AARAMS 1MV Tandemtron. *Radiocarbon* 59(3):905–913. doi: [10.1017/RDC.2016.85](https://doi.org/10.1017/RDC.2016.85).
- Reimer PJ, Baillie MGL, Bard E, Bayliss A, Beck JW, Bertrand CJH, Blackwell PG, Bronk Ramsey C, Buck E, Burr GS, Cutler KP, Damon PE, Edwards RL, Fairbanks RG, Friedrich M, Guilderson TP, Hogg AG, Hughen KA, Kromer B, McCormac FG, Manning SW, Reimer RW, Remmele S, Southon J, Stuiver M, Talamo S, Taylor FW, van der Plicht J, Weyhenmeyer CE. 2004. IntCal04 terrestrial radiocarbon age calibration, 0–26 cal kyr BP. *Radiocarbon* 46(3):1029–1058.
- Reimer PJ, Austin WEN, Bard E, Bayliss A, Blackwell PG, Bronk Ramsey C, Butzin M, Cheng H, Edwards RL, Friedrich M, et al. 2020. The IntCal20 Northern Hemisphere radiocarbon age calibration curve (0–55 cal kyr BP). *Radiocarbon* 62(4):725–757. doi: [10.1017/RDC.2020.41](https://doi.org/10.1017/RDC.2020.41)
- Schulz M, Mudelsee M. 2002. REDFIT: Estimating red-noise spectra directly from unevenly spaced paleoclimatic time series. *Computers & Geosciences* 28(3):421–426. doi: [10.1016/S0098-3004\(01\)00044-9](https://doi.org/10.1016/S0098-3004(01)00044-9).

- Solanki SK, Krivova NA, Schüssler M, Fligge M. 2002. Search for a relationship between solar cycle amplitude and length. *Astronomy and Astrophysics* 396(3):1029–1035. doi: [10.1051/0004-6361:20021436](https://doi.org/10.1051/0004-6361:20021436).
- Southon JR, Magana AL. 2010. A comparison of cellulose extraction and ABA pretreatment methods for AMS  $^{14}\text{C}$  dating of ancient wood. *Radiocarbon* 52(2–3):1371–1379.
- Stuiver M, Braziunas TF. 1993. Sun, ocean, climate and atmospheric  $^{14}\text{CO}_2$ : an evaluation of causal and spectral relationships. *The Holocene* 3(4):289–305.
- Stuiver M, Polach H. 1977. Discussion: reporting of  $\text{C}14$  data. *Radiocarbon* 19(3):355–363.
- Stuiver M, Quay PD. 1980. Changes in atmospheric carbon-14 attributed to a variable Sun. *Science* 207(4426):11–19.
- Stuiver M, Reimer PJ, Braziunas TF. 1998. High-precision radio-carbon age calibration for terrestrial and marine samples. *Radiocarbon* 40(3):1127–1151.
- Tyers I. 1999. DENDRO for Windows program guide. Sheffield, U.K.: University of Sheffield; ARCUS Report 500.
- Usoskin I, Gallet GY, Lopes F, Kovaltsov GA, Hulot G. 2016. Solar activity during the Holocene: the Hallstatt Cycle and its consequence for Grand Minima and Maxima. *Astronomy & Astrophysics* 587(A150):1–10. doi: [10.1051/0004-6361/201527295](https://doi.org/10.1051/0004-6361/201527295).
- Usoskin IG. 2017. A history of solar activity over millennia. *Living Reviews in Solar Physics* 14(3):1–88. doi: [10.1007/s41116-017-0006-9](https://doi.org/10.1007/s41116-017-0006-9).
- Vaquero JM, Gallego MC, Usoskin IG, Kovaltsov GA. 2011. Revisited sunspot data: a new scenario for the onset of the Maunder minimum. *Astrophysical Journal Letters* 731 (L24). doi: [10.1088/2041-8205/731/2/L24](https://doi.org/10.1088/2041-8205/731/2/L24).